Directed assembly of nano-scale phase variants in highly strained BiFeO3 thin films

Jian Zhou, Morgan Trassin, Qing He, Nobumichi Tamura, Martin Kunz, Chun Cheng, Jinxing Zhang, Wen-I Liang , Jan Seidel, Cheng-Lun Hsin, and Junqiao Wu

Citation: Journal of Applied Physics **112**, 064102 (2012); doi: 10.1063/1.4752395
View online: http://dx.doi.org/10.1063/1.4752395
View Table of Contents: http://scitation.aip.org/content/aip/journal/jap/112/6?ver=pdfcov
Published by the AIP Publishing

Directed assembly of nano-scale phase variants in highly strained $BiFeO_3$ thin films

Jian Zhou,[1,a)] Morgan Trassin,[1] Qing He,[2] Nobumichi Tamura,[2] Martin Kunz,[2] Chun Cheng,[1] Jinxing Zhang,[1,b)] Wen-I Liang,[3] Jan Seidel,[4] Cheng-Lun Hsin,[3,c)] and Junqiao Wu[1,4]
[1]*Department of Material Science and Engineering, University of California, Berkeley, California 94720, USA*
[2]*Advanced Light Source, Lawrence Berkeley National Laboratory, Berkeley, California 94720, USA*
[3]*Department of Materials Science and Engineering, National Chiao Tung University, Hsin Chu, Taiwan*
[4]*Materials Sciences Division, Lawrence Berkeley National Laboratory, Berkeley, California 94720, USA*

(Received 26 June 2012; accepted 9 August 2012; published online 17 September 2012)

The delicate balance between elastic energy and electrostatic energy in highly strained $BiFeO_3$ (BFO) thin films results in complex mixed-phase patterns, which poses significant challenges for theoretical understanding and complicates the realization of its full potential in magnetoelectric, electromechanical, and photovoltaic devices. In this letter, we explore in-plane electric field induced phase transition in strain engineered BFO thin films and elucidate the mechanism behind the assembly behavior of complex nano-scale phase domains. Our approach enables deterministic control of phase variants with well-defined structures and orientation, paving the way for designing novel data storage devices based on mixed phase BFO. © *2012 American Institute of Physics*. [http://dx.doi.org/10.1063/1.4752395]

I. INTRODUCTION

In the past decade, much attention has been attracted toward multiferroic materials where two or more ferroic orders coexist, because the coupling between these orders offers the possibility of manipulating magnetic state by an electric field or vice versa.[1–5] Among the few room-temperature multiferroics reported, $BiFeO_3$ (BFO) is the most promising candidate, which shows a wealth of fascinating physical properties, including magnetoelectric coupling,[6–8] domain wall conduction,[9,10] and even photovoltaic effects.[11,12] Recently, large compressive epitaxial strain was successfully achieved in this interesting material, driving the film into a mixture of self-assembled rhombohedral-like (R') phase nano-lamellae embedded in tetragonal–like (T) phase matrix.[13] Moreover, an enhanced spontaneous magnetization of 20-30 emu/cc has been observed in these highly strained R' phase nano-lamellae,[14] making this system extremely attractive for realizing electric-field controlled magnetism. However, in such films, the R' phase nano-lamellae with different morphologies and orientations coexist, and self-assemble into complex bands roughly along two orthogonal, in-plane directions of the film.[13] This is undesirable if the R'-phase lamellae are to be used as nanoscale device elements, such as data storage bits. For example, the spontaneous magnetization of each R' phase lamellae lies along its long axis, and the multiple lamellae orientations result in ambiguity in determining local magnetization easy axis.[14] Therefore, deterministic controlling of *both* the orientation and structure of these R' phase nano-lamellae is necessary for understanding the origin of their magnetization and realizing their potential applications in nano-scale devices.

Previous work by several groups showed that a biased atomic force microscope (AFM) tip with specific probe motion could create R' BFO phases with specific spatial orientations.[15–17] In this report, we discovered the in-plane electric field can direct the nano-sized R' phase lamellae assembly in a unique way, much like the electrically controlled liquid crystal system. We also show that the in-plane electric field creates distinctive R' phase nano-lamellae assembly with single-variant precision, making possible the study of fundamental mechanism driving the complex assembly. Scanning probe microscopy (SPM) combined with synchrotron micro-X ray diffraction (μXRD) techniques were employed to probe the local structural change induced by electrical switching. We find that the T-phase matrix between the R' phase lamellae plays a crucial role in determining the morphology and structure of the R' phase lamellae embedded in it. At last, the spontaneous magnetization in these artificially created R' phase nano-lamellae assembly is investigated by x-ray magnetic circular dichroism (XMCD) based photoemission electron microscopy (PEEM). This reveals that the magnetic easy axis in our system is readily controlled by electric field. Our result represents a critical step towards understanding and ultimate controlling of the spontaneous magnetization in this multiferroic system.

II. EXPERIMENTAL DETAILS

100 nm thick epitaxial thin films of BFO were deposited onto (001) $LaAlO_3$ substrates using pulsed laser deposition at 700 °C in 100 mTorr oxygen atmosphere. The switching electrodes were defined by photolithography, followed by a 50 nm thick gold layer deposition using E-beam metal deposition. To facilitate the R' phase pattern transformation, the samples were heated slightly (to 70 °C) during switching. The μXRD

a)Author to whom correspondence should be addressed. Electronic mail: jackjones@berkeley.edu.
b)Present address: Department of Physics, Beijing Normal University, Beijing, 100875, China.
c)Present address: Department of Electrical Engineering, National Central University, Taoyuan 320, Taiwan.

measurements were performed on Beamline 12.3.2 of the Advanced Light Source. The white spectrum covers an energy range of 5-22 keV. Samples were placed in a reflective geometry at 45° with respect to the incoming beam and diffraction patterns were collected using a Dectris Pilatus 1M detector. The beam spot size is $0.8 \times 1.2\,\mu$m. The patterns were indexed and simulated using the XMAS v6 software package, developed at the ALS by one of us (Tamura). XMCD-PEEM measurements were completed with x-rays that were incident on the sample at an angle of 30° from the surface. Imaging was done by tuning the photon energy to the Fe *L*-edge and using right- or left-handed circularly polarized radiation enabled imaging of the magnetic domain structure by exploiting the XMCD effect at the Fe *L*3- and *L*2-edges.

III. RESULTS AND DISCUSSION

Due to a 4.5% compressive epitaxial strain imposed by the $LaAlO_3$ substrate, different phases coexist in the film: the R' phase with a c/a ratio of 1.1, and the T phase with a c/a ratio of 1.2.[17] Under the AFM, due to their different c/a ratios, T phase is "taller" and appears as a bright matrix, while the R' phase is "shorter" thus appears as dark stripes (Figure 1(a)). The long axes of these R' phase lamellae orient ±15° off the ⟨100⟩ directions of the film as a result of competition between electrostatic and elastic energies.[21] If we draw a line cross-section in Figure 1(a), four different slopes can be found, namely, ±2.8° and ±1.6° (Figure 1(b)). As reported previously[14] and showed here schematically in Figure 1(e), the highly strained R' phase is located under the ±2.8° slopes, while the whole lamella tilts into the region characterized by ±1.6° slope. On the accompanying AFM amplitude image (Figure 1(c)), these two R' phase variants have clear signatures: the variant with positive slope appears bright, while the one with negative slope shows dark contrast. Based on their orientation and structure, eight different basic R' phase variants exist in the as-grown film (Figure 1(d)). They are labeled as variants ①, ②, ③, ④ and ①′, ②′, ③′, ④′. Henceforth, we will use this notation system. The local strain states around these as-grown R' phase nano-lamellae are extremely complicated, making it a great challenge for rigorous theoretical analysis and study.

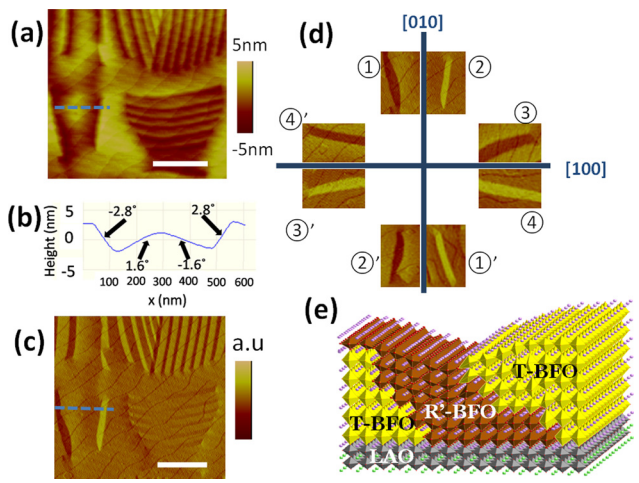

FIG. 1. Eight different R' phase lamellae variants identified in the as-grown film. (a) AFM height image of the BFO sample in as-grown state. T phase is the bright matrix, while the R' phase is the dark stripes. (b) The line-profile across two stripes reveals four distinct surface slopes. (c) The accompanying AFM amplitude image clearly distinguishes the positively and negative slopes on the surface. (d) Eight different basic R' phase variants indentified on the as-grown film. These basic R phase variants orient 15° off the [100] directions. Variant pairs, such as ① and ①′, have the same long axis orientation but opposite surface slope. (e) The schematic for the structure of R' phase nano-lamellae embedded in T phase matrix. The scale bars are all 500 nm.

Recent studies showed complex ferroelectric domains in the as-grown mixed phase BFO film.[16–20,22] A typical AFM morphology and its in-plane piezo-response force microscope (PFM) image of the mixed phase sample are shown in Figures 2(a) and 2(b), which show distinct ferroelectric polarizations. Therefore, understanding the crystal structure and ferroelectric domain structure is the key to control mixed phase pattern by applying electric field. To extract the structural information of the mixed phase region, we performed μXRD studies at the Advanced Light Source (Beamline 12.3.2). The whole Laue diffraction patterns are provided in the supplementary information.[29] For clarity, only the characteristic spots are shown here in Figure 2(d). In the mixed-phase region, four satellite spots around an elongated spot-cluster were observed in the μXRD pattern (Figure 2(d)) (see supplementary information for indexing details),[29] which corresponds to four T phase variants with their c axis tilts along the ⟨110⟩ directions (Figure 2(c)). This is consistent with the four types of ferroelectric domains with polarizations along ⟨110⟩ directions (Figure 2(e)) revealed by PFM scanning in Figure 2(b). After examining the polarization of the T phase domains, we continue to study the polarization of the R' phase nano-lamellae embedded in them. Due to the small width of the R'-phase nano-lamellae (around 50 nm), precise determination of their ferroelectric polarization is hindered by the interference from the phase boundary and adjacent T phase. However, on the in-plane PFM image of the same area with different scanning cantilever directions (Figure S2), we observe the largest in-plane PFM contrast when the scanning cantilever is parallel to the long axis of the R' phase lamellae, and the in-plane PFM contrast decreases monotonically when the angle between the cantilever and R' phase lamellae long axis increases. This suggests that the in-plane polarization projection of the whole R' phase lamellae lies roughly perpendicular to their long axes. This unusual observation could be explained by flexoelectric effect.[23–27] In a ferroelectric system with large strain gradient across the phase boundary,[13] the flexo-electric effect could significantly modify the polarization direction, making it perpendicular to the phase boundary.[27] Each T phase domain is compatible with two R' phase variants, which lie symmetrically about the T phase polarization. We summarize the in-plane polarization projection of the eight R' phase and four T phase variants in Figure 2(f). Based on this chart, selectively nucleating a specific R' phase variant is possible if the ferroelectric domains can be controlled. Realization and identification of the rule of the electric-field selection of R phase variants are an important step toward the ultimate goal of controlled nucleation of any single R' phase variant with electric field. As shown in Figure 2(g), when the electric field is applied along the ⟨−100⟩ direction, the phase variant ① and ② have the same energy gain in the electric field.

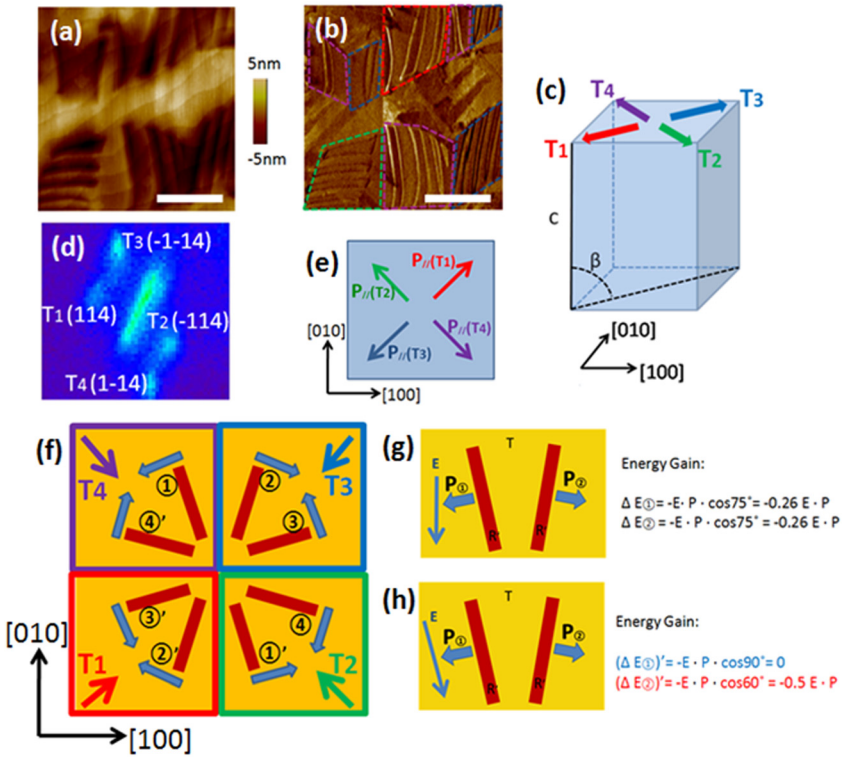

FIG. 2. Ferroelectric domains of mixed phase $BiFeO_3$. (a) AFM height image of the BFO sample in as-grown state. (b) The in-plane ferroelectric domains of the same area as probed by piezo-response force microscope (PFM). The colored dash lines enclose different T phase domains, with the polarization indicated in (e). (d) The micro x-ray diffraction (μXRD) pattern reveals four T-phase variants with the monoclinic distortions along [110] of the pseudo-tetragonal unit cell (c) (see supplementary information).[29] (f) The in-plane polarization projections of the eight R' phase variants are summarized. Each T phase domain is compatible with two specific R' phase variants. The four colored arrows indicate the in-plane polarization projections of T phase domains. (g) An electric field applied along [010] cannot break the degeneracy between R-phase variants ① and ②. (h)This degeneracy can be lifted by applying electric field −15° off [010]. The scale bars in (a) and (b) are 300 nm.

In testing this, a gold electrode based planar capacitor structure was designed to electrically break the in-plane symmetry of the system.[28] Gold electrodes with 1.5 μm spacing were defined on the film by photolithography (Figures 3(a) and S1). Due to the high conformity of the gold layer, it adapts the morphology of the underneath film. The patterns on the electrodes (the areas shadowed by semi-transparent red or green rectangles) are used as position marks. The electric field is at first applied along the [010] direction of the film. After applying a 200 ms, 75 V voltage pulse, the R' phase lamellae pattern is completely modified from its as-grown, natural state (Figures 3(d) and 3(e)). After the

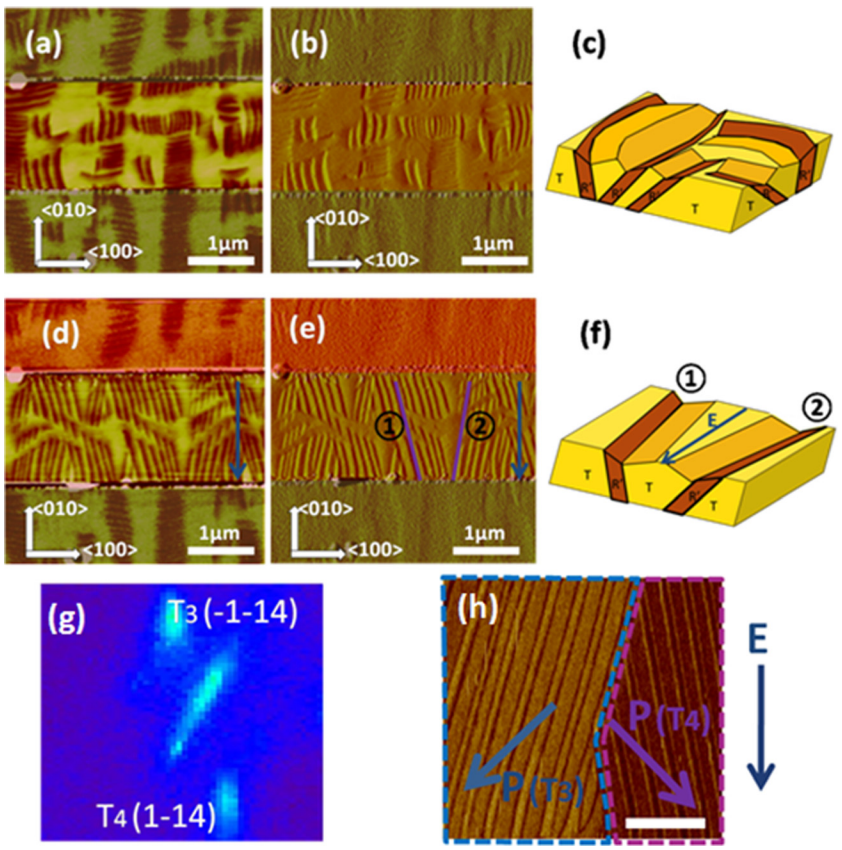

FIG. 3. In-plane electric field induced R' phase variants selection. (a)Line electrodes (the areas shadowed by semi-transparent rectangles) on the film. The accompanying AFM amplitude image and structural schematics are also shown in (b) and (c). (d)-(f) After applying a voltage pulse along the ⟨010⟩ direction, the R' phase lamellae pattern between the electrodes is completely modified, and the number of R-phase variants is reduced from eight to two, which correspond to the R' phase variants ① and ② as previously defined. (g) The μXRD pattern of the area after electric switching. Note: T phase variants T1 and T2 are absent after electric switching. (h) The ferroelectric domains of the switched sample. In accordance with (g), only two T phase ferroelectric domains (T3 and T4) are observed. The blue arrows indicate the direction of the applied electric field, the scale bar is 300 nm.

electrical switching, the number of R' phase variants is greatly reduced from eight to two, which correspond to R' phase variants ① and ② as previously defined in Figure 1(b). On the accompanying AFM amplitude images (Figure 3(b) and 3(e)), we also determine the local slope on the surface. Combining the information derived from the AFM height and amplitude images, we are able to draw structural schematics of the R' phase lamellae before and after the electrical switching (Figures 3(c) and 3(f)). By reversing the polarity of this switching electric field, the mixed phase pattern between the electrodes is modified again and the other two R' phase variants emerge (Figure S4), which correspond to ①′ and ②′ as previously defined. This can be readily explained by Figure 2(f). When the E field is along the $\langle 0-10\rangle$ direction (as in Figure 3(d)), the T phase domains T1 and T2 are eliminated because their polarizations are opposing the applied electric field; the R' phase variants ①′, ②′, ③′, and ④ are also de-selected in this step. Only T phase domains of T3 and T4 remain, and R' phase variants ①, ②, ③, and ④′ are compatible with them. Taking into account the in-plane polarization of the R phase lamellae, we further find R' phase variants ③ and ④′ are also unfavorable because their in-plane polarizations oppose the applied electric field. On the other hand, R' phase variants ① and ② are energetically preferred in this artificially created electrostatic environment, thus they become the only two R' phase variants filtered by the electric field switching. This is further supported by the μXRD and PFM study of the area after in-plane electric field switching (Figures 3(g) and 3(h)), in which only two T phase variant remains—reminiscent to conventional ferroelectric domain switching.

Such a result evidences the success of our design rules and further suggests a single phase variant selection strategy. Applying an electric field slightly off [100] can effectively further break this degeneracy (Figure 2(h)). As a simple estimation, we assume that the in-plane polarization component of R' phase lamellae ① and ② is P. When the electric field is applied along 15° off the $\langle 010\rangle$, the electrostatic energy difference between these two R' phase lamellae is as large as 0.5E·P. In order to achieve this, the in-plane electrode were oriented so that the applied in-plane electric field tilts ±15° away from the [010] directions, as shown in Figures 4(a) and 4(d). After applying an electric field along −15° off the $\langle 010\rangle$ direction (i.e., along the long axis of R' phase variant ①), all the re-nucleated R' phase lamellae are aligned in the same direction +15° away from the [010] direction (Figure 4(a)). Interestingly, on the accompanied AFM amplitude image (Figure 4(b)), all the R' phase lamellae appear bright, which indicates their top surfaces all tilt to the left-hand side of the page. According to our notation system in Figure 1(b), all the R' phase lamellae between the electrodes belong to variant ②. This is exactly predicted by our analysis in Figure 2(h): due to the in-plane polarization component of the R' phase lamellae, variant ② is energetically more favorable than variant ① under this switching filed. Applying the same voltage pulse but in the opposite direction, the AFM amplitude contrast of the re-nucleated R' phase lamellae is reversed (Figure 4(d)), which indicates that their top surfaces tilt to the right-hand side of the page, showing that now variant ②′ is successfully nucleated, evidencing our ability to switch between the two different R' phase variants with electric field of opposite polarities. Other variants can also be nucleated and transformed in a similar fashion (Figure S5).

The artificially created single R' phase variant provides an ideal system for studying the correlation between local strain state and spontaneous magnetization in highly strained

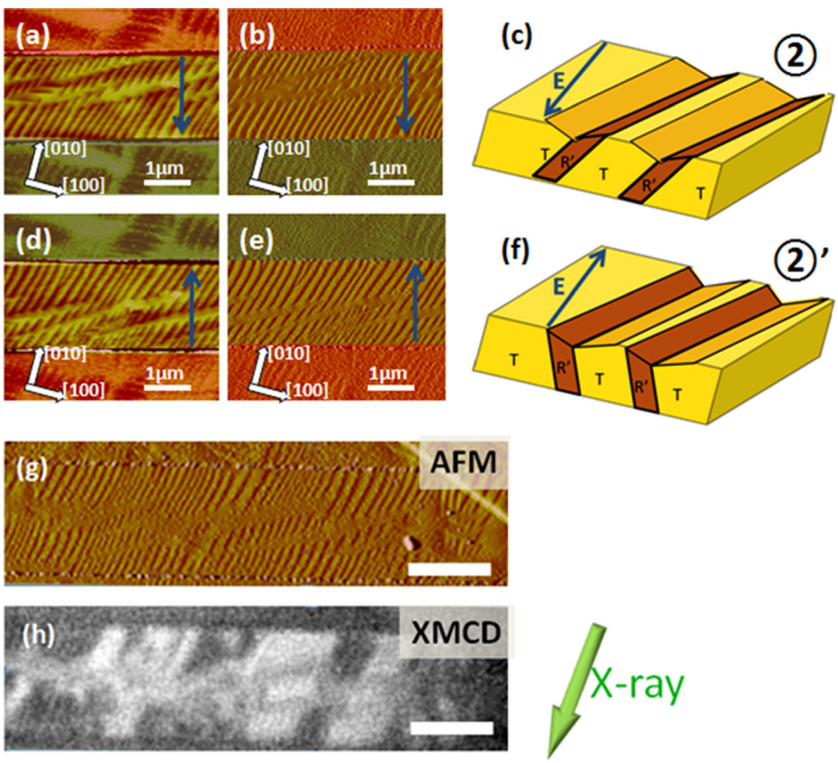

FIG. 4. Deterministically control the phase variants assembly and probing their magnetic properties. (a)-(f) By applying electric field 15° off [010], single R' phase variant assembly can be deterministically created. (a)-(c) creation of phase variant ②. (d)-(e) creation of phase variant ②′. AFM amplitude images (b) and (e) indicate these two R' phase variant have opposite surface slope. Other variants can also be individually addressed in similar fashion. The blue arrows indicate the direction of the applied electric field. (g) The AFM amplitude image of an ensemble of electrically created R' phase variant ②′. All the R' phase variants have the same orientation and structure. (h) XMCD image of exactly the same area. The incident x-ray wave vector (the green arrow on the side) is along the long axes of R' phase lamellae. The image contrast is effectively a map of the local magnetization vectors; regions with magnetic moment lying parallel to the x-ray wave vector show bright contrast, while those that are antiparallel appear in dark contrast. The areas without R' phase lamellae (pure T phase) shows neutral gray contrast. Unlike the as-grown film, the magnetic easy axis is well defined in the artificially selected system, which is along the long axis of these R' phase nano-lamellae. The scale bars in (g) and (h) are 1 μm.

BFO films. As shown in Ref. 14, the spontaneous magnetization of the R phase nano-lamellae is always along their long axis, which means that the magnetic easy axis is readily defined in our electrically switched samples in Figures 4(a) and 4(d). In the as-grown film, different R' phase variants coexist or even join together to form compound R' phase lamellae, leading to extremely complex local strain state. However, our artificially created single R' phase variant assembly greatly simplifies this complexity: a single R' phase variant with well-defined structure and orientation embedded in T phase matrix of specific ferroelectric polarization. The weak ferromagnetism in BFO films is highly correlated to its local structural distortions,[7] and electric-field induced magnetization reversal is possible if the local structure and ferroelectric order are well controlled. In order to study the magnetic response of these electrically created single variant R' phase pattern, XMCD based PEEM was used to image the magnetic domains. Figures 4(g) and 4(h) are the AFM amplitude and PEEM magnetism images of the same switched area of a BFO sample. All the R' phase lamellae with the same structure are assembled along the same direction after the electric field switching (Figure 4(g)). The XMCD-PEEM measurement shown in Figure 4(h) displays a unique magnetic easy axis which is along the long axes of R-phase nano-lamellae, the spontaneous magnetization of the R-phase lamellae is either parallel (bright contrast) or antiparallel (dark contrast) to the direction of the incident x-ray. It is expected that our results can stimulate further theoretical study about the structure-correlated enhanced magnetism in these highly strained R' phase nano-lamellae.

IV. CONCLUSIONS

By applying an in-plane electric field, we have realized deterministic control of R' phase domains in strain engineered BFO epitaxial layers, which sheds light on the mechanism of R' phase lamellae assembly. Our results show that the T-phase matrix between the R' phase lamellae play a crucial role in determining the morphology and structure of the R' phase lamellae embedded in it. We also demonstrate that the degeneracy of the R' phase variants can be lifted by applying an electric field along specific angles. Our approach provide a reliable route for electrically manipulating the R' phase nano-lamellae that carry enhanced magnetic moments, hence paving the way toward designing novel nano-scale magnetoelectric data storage devices.

ACKNOWLEDGMENTS

The device fabrication and AFM measurements were supported by a NSF CAREER Award under Grant No. DMR-1055938. The μXRD measurements were performed at the Advanced Light Source of the Lawrence Berkeley National Laboratory, which is supported by the Office of Science, Office of Basic Energy Sciences, Scientific User Facilities Division, of the U.S. Department of Energy under Contract No. DE-AC02—05CH11231. The micro-diffraction indexing program at the ALS on BL 12.3.2 was made possible by NSF Grant No. 0416243. We thank Prof. Y. H. Chu in National Chiao Tung University, Taiwan for thoughtful discussions. We thank Professor R. Ramesh in UC Berkeley for help in material preparation.

[1]W. Eerenstein, N. D. Mathur, and J. F. Scott, Nature **442**, 759–765 (2006).
[2]N. A. Spaldin and M. Fiebig, Science **309**, 391–392 (2005).
[3]M. Mostovoy, Phys. Rev. Lett. **96**, 067601 (2006).
[4]D. I. Khomskii, J. Magn. Magn. Mater. **306**, 1–8 (2006).
[5]S.-W. Cheong and M. Mostovoy, Nature Mater. **6**, 13–20 (2007).
[6]Y.-H. Chu, L. W. Martin, M. B. Holcomb, G. Martin, S. Han, Q. He, N. Balke, C. H. Yang, D. Lee, W. Hu *et al.* Nature Mater. **7**, 478–482 (2008).
[7]C. Ederer and N. A. Spaldin, Phys. Rev. B **71**, 060401 (2005).
[8]A. M. Kadomtseva, A. K. Zvezdin, Y. F. Popov, A. P. Pyatakov, and G. P. Vorob'ev, JETP Lett. **79**, 571–581 (2004).
[9]J. Seidel, L. W. Martin, Q. He, Q. Zhan, Y.-H. Chu, A. Rother, M. E. Hawkridege, P. Maksymovych, P. Yu, M. Gajek *et al.*, Nature Mater. **8**, 229–234 (2009).
[10]J. Seidel, P. Maksymovych, Y. Batra, A. Katan, S.-Y. Yang, Q. He, A. P.Baddorf, S. V. Kalinin, C.-H. Yang, J.-C.Yang *et al.*, Phys. Rev. Lett. **105**, 197603 (2010).
[11]T. Choi, S. Lee, Y. J. Choi, V. Kiryukhin, and S.-W. Cheong, Science **324**, 63–66 (2009).
[12]S. Y. Yang, J. Seidel, S. J. Byrnes, P. Shafer, C.-H. Yang, M. D. Rossell, P. Yu, Y.-H. Chu, J. F. Scott, J. W. Ager *et al.*, Nature Nanotechnol. **5**, 143–147 (2010).
[13]R. J. Zeches, M. D. Rossell, J. X. Zhang, A. J. Hatt, Q. He, C.-H. Yang, A. Kumar, C. H. Wang, A. Melville, C. Adamo *et al.*, Science **326**, 977–980 (2009).
[14]Q. He, Y. -H. Chu, J. T. Heron, S. Y. Yang, W. I. Liang, Kuo, C. Y. H. J. Lin, P. Yu, C. W Liang, R. J. Zeches *et al.*, Nat. Commun. **2**, 225 (2011).
[15]R. K. Vasudevan, Y. Liu, J. Li, W. I. Liang, A. Kumar, S. Jesse, Y. C. Chen, Y. H. Chu, V. Nagarajan and S. V. Kalinin,Nano. Lett. **11**, 3346–3354 (2011).
[16]Y. C. Chen, Q. He, F. N. Chu, Y. C. Huang, J. W. Chen, W. I. Liang, R. K. Vasudevan, V. Nagarajan, E. Arenholz, S. V. Kalinin, and Y. H. Chu, Adv. Mater. **24**, 3070–3075 (2012).
[17]L. You, Z. Chen, X. Zou, H. Ding, W. Chen, L. Chen, G. Yuan, and J. Wang, ACS Nano **6**(6), 5388–5394 (2012).
[18]For simplicity, we follow the convention in literatures to label these phases as "R'" and "T". Strictly speaking, as discussed in Refs. 19 and 20, both R' phase and T-like phase are monoclinic phases, but with different lattice parameters and monoclinic angles. For clarity, we restrict our discussion of the "T phase" in the mixed phase region (between adjacent R' phase lamella) in this paper. The "T phase" outside the mixed phase region is well studied and was identified as Mc phases[19,20] but is different from the "T phase" inside the mixed phase region, which is more close to MA phase (from our micro-XRD data).
[19]A. R. Damodaran, C.-W. Liang, Q. He, C.-Y. Peng, L. Chang, Y.-H. Chu, and L. W. Martin, Adv. Mater. **23**, 3170–3174 (2011).
[20]Z. H. Chen, Z. L. Luo, C. W. Huang, Y. Qi, P. Yang, L. You, C. Hu, T. Wu, J. L. Wang. C. Gao *et al.*, Adv. Funct. Mater. **21**, 133–138 (2011).
[21]C. W. Huang, Y. H. Chu, Z. H. Chen, J. Wang, T. Sritharan, Q. He, R. Ramesh, and L. Chen, Appl. Phys. Lett. **97**, 152901 (2010).
[22]D. Mazumdar, V. Shelke, M. Iliev, S. Jesse, A. Kumar, S. V. Kalinin, A. P. Baddorf, and A. Gupta, Nano Lett. **10**, 2555–2561 (2010).
[23]G. Catalan, L. J. Sinnamon, and J. M. Gregg, J. Phys. Condens. Matter **16**, 2253–2264 (2004).
[24]G. Catalan, B. Noheda, J. McAneney, L. J. Sinnamon, and J. M. Gregg, Phys. Rev. B **72**, 020102 (2005).
[25]L. E. Cross, J. Mater. Sci. **41**, 53–63 (2006).
[26]W. Ma, Phys. Status Solidi B. **245**, 761–768 (2008).
[27]G. Catalan, A. Lubk, A. H. G.Vlooswijk, E. Snoeck, C. Magen, A. Janssens, G. Rispens, G. Rijnders, D. H. A. Blank, and B. Noheda, Nature Mater. **10**, 963–967 (2011).
[28]N. Balke, M. Gajek, A. K. Tagantsev, L. W. Martin. Y. H. Chu, R. Ramesh, S. V. Kalinin, Adv. Funct. Mater. **20**, 3466–3475 (2010).
[29]See supplementary material at http://dx.doi.org/10.1063/1.4752395 for device fabrication, more comprehensive planar electrode switching, micro-X ray diffraction and X-ray magnetic circular dichroism.